AFRL-VA-WP-TR-1998-3080

NEW CONTROL DESIGN TECHNIQUES TAILORED TO SMART STRUCTURAL SYSTEMS

R.K. YEDAVALLI

OHIO STATE UNIVERSITY
DEPT OF AEROSPACE ENGINEERING, APPLIED MECHANICS, & AVIATION
2036 NEIL AVENUE
COLUMBUS, OH 43210-1276

NOVEMBER 1998

FINAL REPORT FOR 05/05/1997 – 06/05/1998

AIR VEHICLES DIRECTORATE
AIR FORCE RESEARCH LABORATORY
AIR FORCE MATERIEL COMMAND
WRIGHT-PATTERSON AIR FORCE BASE OH 45433-7542

NOTICE

USING GOVERNMENT DRAWINGS, SPECIFICATIONS, OR OTHER DATA INCLUDED IN THIS DOCUMENT FOR ANY PURPOSE OTHER THAN GOVERNMENT PROCUREMENT DOES NOT IN ANY WAY OBLIGATE THE US GOVERNMENT. THE FACT THAT THE GOVERNMENT FORMULATED OR SUPPLIED THE DRAWINGS, SPECIFICATIONS, OR OTHER DATA DOES NOT LICENSE THE HOLDER OR ANY OTHER PERSON OR CORPORATION; OR CONVEY ANY RIGHTS OR PERMISSION TO MANUFACTURE, USE, OR SELL ANY PATENTED INVENTION THAT MAY RELATE TO THEM.

THIS REPORT IS RELEASABLE TO THE NATIONAL TECHNICAL INFORMATION SERVICE (NTIS). AT NTIS, IT WILL BE AVAILABLE TO THE GENERAL PUBLIC, INCLUDING FOREIGN NATIONS.

THIS TECHNICAL REPORT HAS BEEN REVIEWED AND IS APPROVED FOR PUBLICATION.

Nelson D. Wolf

NELSON D. WOLF, Chief
Design and Analysis Branch
Structures Division

Duane E. Veley

DUANE E. VELEY
Design and Analysis Branch
Structures Division

J. M. Manter

JOSEPH M. MANTER
Chief
Structures Division

Do not return copies of this report unless contractual obligations or notice on a specific document requires its return.

REPORT DOCUMENTATION PAGE	Form Approved OMB No. 0704-0188

1. AGENCY USE ONLY *(Leave blank)*	2. REPORT DATE	3. REPORT TYPE AND DATES COVERED
	NOVEMBER 1998	FINAL REPORT FOR 05/05/1997 - 06/05/1998

4. TITLE AND SUBTITLE
NEW CONTROL DESIGN TECHNIQUES TAILORED TO SMART STRUCTURAL SYSTEMS

5. FUNDING NUMBERS
C F33615-97-1-3207
PE 61102
PR 2302
TA N5
WU 0A

6. AUTHOR(S)
R.K. YEDAVALLI

7. PERFORMING ORGANIZATION NAME(S) AND ADDRESS(ES)
OHIO STATE UNIVERSITY
DEPT OF AEROSPACE ENGINEERING, APPLIED MECHANICS AND AVIATION
2036 NEIL AVENUE
COLUMBUS, OH 43210-1276

8. PERFORMING ORGANIZATION REPORT NUMBER

9. SPONSORING/MONITORING AGENCY NAME(S) AND ADDRESS(ES)
AIR VEHICLES DIRECTORATE
AIR FORCE RESEARCH LABORATORY
AIR FORCE MATERIEL COMMAND
WRIGHT-PATTERSON AFB, OH 45433-7542
POC: DUANE VELEY, AFRL/VASD, 937-255-6434

10. SPONSORING/MONITORING AGENCY REPORT NUMBER
AFRL-VA-WP-TR-1998-3080

11. SUPPLEMENTARY NOTES

12a. DISTRIBUTION AVAILABILITY STATEMENT
APPROVED FOR PUBLIC RELEASE; DISTRIBUTION IS UNLIMITED

12b. DISTRIBUTION CODE

13. ABSTRACT *(Maximum 200 words)*

In this research, a new observer based control design specifically tailored to smart aerooelastic systems is presented. This truly multi-disciplinary system of an elastic structure with piezoelectric actuating and sensing under external aerodynamic load is modeled with an integrated finite element method. A new control design algorithm based on 'Reciprocal State Space' framework is developed to achieve the desired roll rate. The deformed structure for obtaining the specific roll rate is made up of new mass and stiffness matrices which are functions of the steady-state input voltage of the roll maneuver. The resulting model in the generalized coordinates which has a mass matrix, a nonsymmetric aerodynamic damping matrix and a nonsymmetric stiffness matrix (due to aerodynamic stiffness) is then transformed to real but nonorthogonal modal coordinates and a reduced order model is developed. The research carried out clearly delineates the relationship and interaction between the structural, aerodynamic and piezo actuations based control subsystems and underscores the importance, potential and the vast scope of the integrated approach presented to improve aircraft maneuver performance.

14. SUBJECT TERMS	15. NUMBER OF PAGES
PIEZOELECTRIC, SMART STRUCTURES, AERODYNAMICS, CONTROLS, RECIPROCAL STATE SPACE	47
	16. PRICE CODE

17. SECURITY CLASSIFICATION OF REPORT	18. SECURITY CLASSIFICATION OF THIS PAGE	19. SECURITY CLASSIFICATION OF ABSTRACT	20. LIMITATION OF ABSTRACT
UNCLASSIFIED	UNCLASSIFIED	UNCLASSIFIED	SAR

Table of Contents

List of Figures

PREFACE

This report was prepared by the Department of Aerospace Engineering, Applied Mechanics and Aviation, The Ohio State University, Columbus, OH, 43210, under the U.S. Air Force Material Command Grant F33615-97-1-3207. The work was performed under the direction of Dr. Narendra Khot of the Design and Analysis Branch, Structures Division, Air Force Research Laboratory(AFRL/VASD).

The technical work was conducted by Dr. R. K. Yedavalli, Principal Investigator and Graduate Assistant Mr. Seung-Keon Kwak. The Grant work was performed during the period Apr 1997 - May 1998.

The investigators in this study wish to thank Dr. Narendra Khot for his guidance and support.

1 Introduction:

In nature, birds change their wing shapes to achieve proper flight performance. Humans have long pursued the dream of achieving bird-like flight performance. Efforts in that direction led to the development of rigid control surfaces such as an elevator, ailerons, a rudder, and flaps for conventional aircraft. However these efforts were only adequate for limited flight envelops and maneuvers. Many modern fighter aircraft are required to possess rapid maneuverability at high speeds. If one attempts to accomplish this with traditional control surfaces, many difficulties arise. One of them is the roll reversal phenomenon and the other is the vibration problem. During a swift roll motion, wings are deformed significantly due to high dynamic pressure. In recent years, therefore, design and control of a deformable wing based on smart structure actuation and sensing has become an active topic of research in the aerospace community. A properly deformable wing structure is expected to enable the aircraft to have faster and gentler maneuver as well as more efficient and safer performance (like that of a bird) by using the interaction among the elastic structures, smart materials, and external aerodynamic pressure. Federal Research Laboratories such as Wright Laboratory, DARPA, and industries such as Northrop Grumman are actively engaged in research and development of this challenging multidisciplinary area with extensive applications [1][2].

Most of the previous modeling and control design research in this multidisciplinary area is confined to integration of any two subdisciplines such as structures and control, control and smart materials, structures and smart materials. Only recently the truly integrated problem of incorporating all four subdisciplines, namely structures, aerodynamics, smart materials and control system design is being attempted. This type of pure and straightforward integration of these four disciplines is realized to be a complicated task requiring expertise in all of these disciplines. In addition, for applications involving aircraft maneuvers one should even add another subdiscipline, namely flight mechanics! One of the first attempts to incorporate structures, aerodynamics, control and flight mechanics (addressing specifically the roll maneuver) are the series of papers by WL and Northrop Grumman researchers Khot, Eastep, Kari Appa and their colleagues [3][4]. In research presented in this report, an attempt is made, perhaps for the first time, to achieve integration of all the above five disciplines! In this research, efforts are undertaken to model and control the aeroelastic dynamics of a flexible wing structure embedded with piezo material for actuation and

sensing so that a roll maneuver with a desired roll rate is achieved by actively deforming the wing.

Typically, the motion of the multi-disciplinary flexible aircraft structures, such as a piezo-laminated aircraft structure in aerodynamic field[5], can be expressed in the form of multi-variable linear ordinary second order differential equation in the 'configuration or generalized' coordinates in the form of the well known 'Matrix Second Order (MSO)' system framework involving Mass, Damping and Stiffness matrices. The pure structural system, generally, consists of a constant symmetric positive definite and a positive semi-definite mass and stiffness matrices, respectively. The multi-disciplinary flexible aircraft structural system, however, is formed with a symmetric positive definite mass matrix but a nonsymmetric and indefinite damping (which includes aerodynamic damping) and stiffness (that includes aerodynamic and piezo material stiffness, in addition to the standard structural stiffness) matrices. For flight mechanics problems, the static deformation of the wing is essential to obtain desired performance of the aircraft. Thus, deformed structural mass, damping, and stiffness matrices, which are functions of the steady- state voltage input for obtaining the desired flight maneuver is also included in the control design model.

The piezoelectric voltages serve as the control variables. To have constant roll rate, a new framework called 'Reciprocal State Space' framework is used for control design purposes. This new modeling and control design methodology is illustrated with the help of an example and its efficacy clearly demonstrated. First, the large model for the deformed structural dynamics in the generalized coordinates is transformed to a set of 'nonorthogonal modal' coordinates and model reduction is carried out in these modal coordinates. Typically, this model is then converted to the 'state space' form and a control design algorithm is developed treating the problem as a regulation problem.

The resulting full state and state derivative feedback controller is possible only when every state and state derivative measurements are available. Practically, however, it is impossible to measure all the states and their derivatives. For example, the piezo-laminated aircraft structure in aerodynamic field provides only displacement information through piezoelectric sensors. Thus, an observer is required to design a proper feedback controller. Traditionally, the observers are designed in the first order state-space framework. However, there are several noticeable problems in the first order observer that is designed by converting a second order system to a first order state space form. In this research, therefore, a new second order observer design is presented to

obtain improved controller performance as well as to determine the minimum number and location of the sensors. In the next section we present the details of the integrated modeling for control design purposes.

2 Integrated Modeling for Smart Flexible Deformable Wings:

In Kari Appa, Khot, et al. [6], the matrix second order equations of motion are first derived using the 'orthogonal modal' coordinates of the pure structural dynamic system, and the aerodynamic pressure distribution to achieve roll motion is assumed to be known along these 'modal coordinates', which is the typical procedure currently followed by most aeroelastic studies. However, in this research, attempts are made to obtain a more generic model that is applicable not only to the present problem of roll maneuvers but also to the future applications involving pitch, roll and yaw maneuvers. With this in mind, it is argued that this type of generic maneuver model can be developed easier in the 'generalized' coordinates rather than in the orthogonal modal coordinates. In the orthogonal modal coordinate approach, it is difficult to simultaneously consider the influence or coupling of the other subsystems such as aerodynamics, controls, flight mechanics and smart material actuation and sensing whereas this is possible in the direct 'generalized' coordinates. Of course there is a price to be paid later for this generality! It is that when model reduction is required for control design, the necessary step of converting to the modal coordinates involves 'nonorthogonal' modal coordinates! However, it is felt that this is a smaller price to pay considering the 'true integration' achieved when modeling is done in the 'generalized' coordinates. So in what follows, we develop a finite element model with nodal displacements as the 'generalized' coordinates and simultaneously incorporate the aerodynamic pressure distribution as well as piezo actuation directly integrated into this finite element model.

2.1 Finite Element Modeling of a Smart Material (Piezoelectric) Wing Subject to Aerodynamic Loads:

The constitutive equations for a piezoelectric material are expressed as [7]

$$\{\mathbf{T}\} = [\mathbf{c}]\{\mathbf{S}\} - [\mathbf{e}]^T\{\mathbf{E}\} \tag{1}$$

$$\{\mathbf{D}\} = [\mathbf{e}]\{\mathbf{S}\} + [\epsilon]\{\mathbf{E}\} \tag{2}$$

where

$$\{\mathbf{T}\} = [\sigma_{xx}\ \sigma_{yy}\ \sigma_{zz}\ \sigma_{yz}\ \sigma_{zx}\ \sigma_{xy}]^T\ ; stress\ vector$$

$$\{\mathbf{S}\} = [\varepsilon_{xx}\ \varepsilon_{yy}\ \varepsilon_{zz}\ \gamma_{yz}\ \gamma_{zx}\ \gamma_{xy}]^T \text{ ; strain vector}$$

$$\{\mathbf{E}\} = [E_x\ E_y\ E_z]^T \text{ ; electric field vector}$$

$$\{\mathbf{D}\} = [D_x\ D_y\ D_z]^T \text{ ; electric displacement vector}$$

$$[\mathbf{c}] = \begin{bmatrix} C_{11} & C_{12} & C_{13} & 0 & 0 & 0 \\ C_{12} & C_{11} & C_{13} & 0 & 0 & 0 \\ C_{13} & C_{13} & C_{33} & 0 & 0 & 0 \\ 0 & 0 & 0 & C_{44} & 0 & 0 \\ 0 & 0 & 0 & 0 & C_{44} & 0 \\ 0 & 0 & 0 & 0 & 0 & C_{44} \end{bmatrix}$$

$$[\mathbf{e}] = \begin{bmatrix} 0 & 0 & 0 & 0 & e_{15} & 0 \\ 0 & 0 & 0 & e_{24} & 0 & 0 \\ e_{31} & e_{32} & e_{33} & 0 & 0 & 0 \end{bmatrix}$$

$$[\epsilon] = \begin{bmatrix} \epsilon_{11} & 0 & 0 \\ 0 & \epsilon_{11} & 0 \\ 0 & 0 & \epsilon_{33} \end{bmatrix}$$

2.2 Finite Element Model using Coupled 8-node Brick Elements

In order to generate the finite element formulation of a flexible wing, 8-node coupled brick elements(Fig. 1) are employed. The shape functions of the elements are expressed as

$$N_i = \frac{1}{8}(1+\xi\xi_i)(1+\eta\eta_i)(1+\zeta\zeta_i) \tag{3}$$

Each node of the element has 4 degrees of freedom which are spatial displacements(u, v, w) and voltage($\mathbf{V}$). These displacements and voltage are coupled to each other according to the constitutive equation (Eq. 2). The displacement fields with the shape functions in the finite element model are expressed as

$$\mathbf{u} = [\mathbf{N}_q]\{q_i\} = [\mathbf{N}_q]\mathbf{q} \tag{4}$$

$$\varphi = [\mathbf{N}_\varphi]\{v_i\} = [\mathbf{N}_\varphi]\mathbf{v} \tag{5}$$

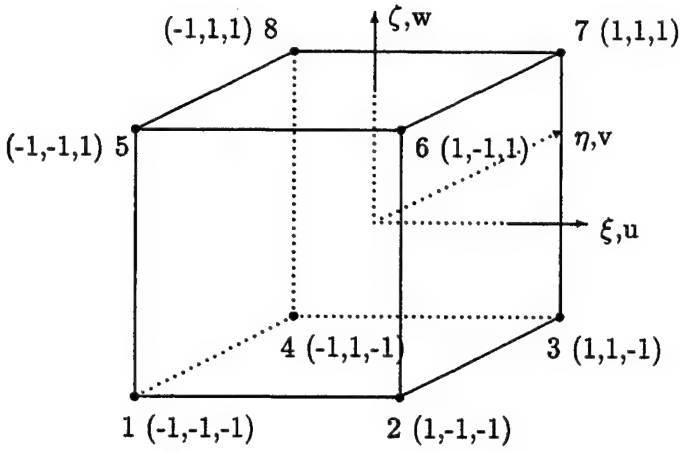

Figure 1: Coupled 8 Nodes 3-D Solid

where

$$[\mathbf{N}_q] = \begin{bmatrix} N_1 & 0 & 0 & N_2 & 0 & 0 & N_3 & 0 & 0 & \dots \\ 0 & N_1 & 0 & 0 & N_2 & 0 & 0 & N_3 & 0 & \dots \\ 0 & 0 & N_1 & 0 & 0 & N_2 & 0 & 0 & N_3 & \dots \end{bmatrix}$$

$$[\mathbf{N}_\varphi] = \begin{bmatrix} N_1 & N_2 & N_3 & \dots \end{bmatrix}$$

$$[\mathbf{q}] = \begin{bmatrix} u_1 & v_1 & w_1 & u_2 & v_2 & w_2 & u_3 & v_3 & w_3 & \dots \end{bmatrix}^T$$

$$[\varphi] = \begin{bmatrix} V_1 & V_2 & V_3 & \dots \end{bmatrix}^T$$

Then, the strain and electric fields are written as

$$\mathbf{S} = [\mathbf{L}_q][\mathbf{N}_q]\{q_i\} = [\mathbf{B}_q]\mathbf{q} \tag{6}$$

$$\mathbf{E} = [\mathbf{L}_\varphi][\mathbf{N}_\varphi]\{\varphi_i\} = [\mathbf{B}_\varphi]\varphi \tag{7}$$

where

$$[\mathbf{B}_q] = \begin{bmatrix} \frac{\partial N_1}{\partial \xi} & 0 & 0 & \frac{\partial N_2}{\partial \xi} & 0 & 0 & \frac{\partial N_3}{\partial \xi} & 0 & 0 & \cdots \\ 0 & \frac{\partial N_1}{\partial \eta} & 0 & 0 & \frac{\partial N_2}{\partial \eta} & 0 & 0 & \frac{\partial N_3}{\partial \eta} & 0 & \cdots \\ 0 & 0 & \frac{\partial N_1}{\partial \zeta} & 0 & 0 & \frac{\partial N_2}{\partial \zeta} & 0 & 0 & \frac{\partial N_3}{\partial \zeta} & \cdots \\ 0 & \frac{\partial N_1}{\partial \zeta} & \frac{\partial N_1}{\partial \eta} & 0 & \frac{\partial N_2}{\partial \zeta} & \frac{\partial N_2}{\partial \eta} & 0 & \frac{\partial N_3}{\partial \zeta} & \frac{\partial N_3}{\partial \eta} & \cdots \\ \frac{\partial N_1}{\partial \zeta} & 0 & \frac{\partial N_1}{\partial \xi} & \frac{\partial N_2}{\partial \zeta} & 0 & \frac{\partial N_2}{\partial \xi} & \frac{\partial N_3}{\partial \zeta} & 0 & \frac{\partial N_3}{\partial \xi} & \cdots \\ \frac{\partial N_1}{\partial \eta} & \frac{\partial N_1}{\partial \xi} & 0 & \frac{\partial N_2}{\partial \eta} & \frac{\partial N_2}{\partial \xi} & 0 & \frac{\partial N_3}{\partial \eta} & \frac{\partial N_3}{\partial \xi} & 0 & \cdots \end{bmatrix}$$

$$[\mathbf{B}_\varphi] = \begin{bmatrix} \frac{\partial N_1}{\partial \xi} & \frac{\partial N_2}{\partial \xi} & \frac{\partial N_3}{\partial \xi} & \cdots \\ \frac{\partial N_1}{\partial \eta} & \frac{\partial N_2}{\partial \eta} & \frac{\partial N_3}{\partial \eta} & \cdots \\ \frac{\partial N_1}{\partial \zeta} & \frac{\partial N_2}{\partial \zeta} & \frac{\partial N_3}{\partial \zeta} & \cdots \end{bmatrix}$$

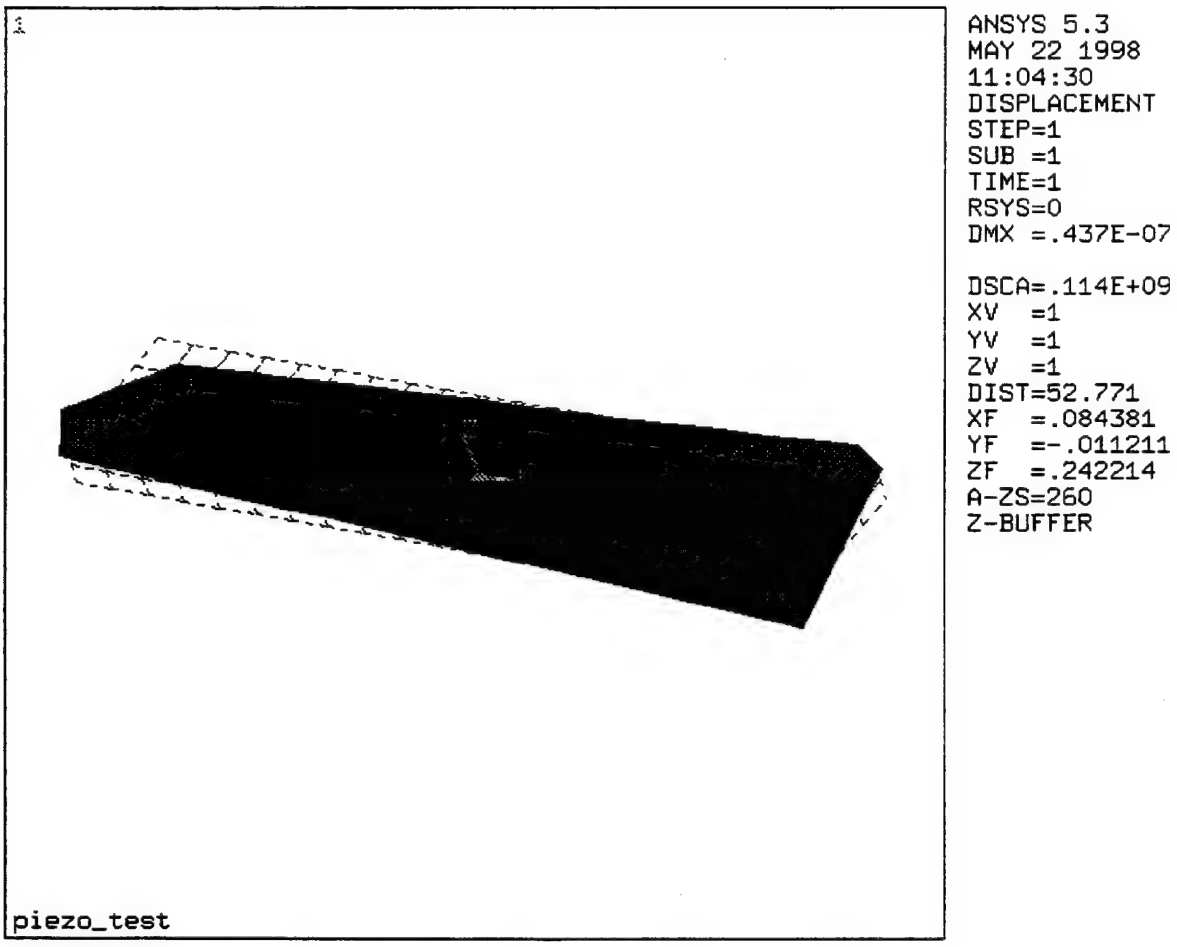

Figure 2: A Twisting Motion in a Flexible Wing

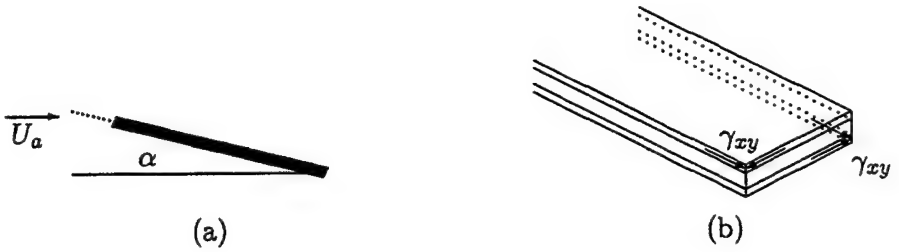

Figure 3: Torsional Motion of Cross Section of a Wing

2.3 Torsional Motion of Piezo-electric Continua

Since lift forces are varied by changing the angle of attack, α, of a wing, which in turn can be changed by the twisting motion of the wing, it is clear that we need to impart twisting motion to the wing to be able to generate the required moments for various flight maneuvers such as roll. Fig. 3(a) and Fig. 2 show angle of attack and twisting motion of a wing, respectively. A pair of shear strains, γ_{xy}, in opposite direction are needed to produce twisting moment of wing as shown in Fig. 3(b). The directional attachment technique of the piezoelectric actuators [8] is employed to achieve twisting motion of the wing. From Fig. 4, the relation between the principal axes and reference axes is expressed as

$$\{\mathbf{T}'\} = [\mathbf{T}_t]\{\mathbf{T}\} \tag{8}$$

$$\{\mathbf{S}'\} = [\mathbf{T}_s]\{\mathbf{S}\} \tag{9}$$

where

$$[\mathbf{T}_t] = \begin{bmatrix} l_1^2 & m_1^2 & n_1^2 & 2m_1n_1 & 2n_1l_1 & 2l_1m_1 \\ l_2^2 & m_2^2 & n_2^2 & 2m_2n_2 & 2n_2l_2 & 2l_2m_2 \\ l_3^2 & m_3^2 & n_3^2 & 2m_3n_1 & 2n_3l_1 & 2l_3m_1 \\ l_2l_3 & m_2m_3 & n_2n_3 & m_2n_3+m_3n_2 & l_2n_3+l_3n_2 & l_2m_3+l_3m_2 \\ l_1l_3 & m_1m_3 & n_1n_3 & m_1n_3+m_3n_1 & l_1n_3+l_3n_1 & l_1m_3+l_3m_1 \\ l_2l_1 & m_2m_1 & n_2n_1 & m_2n_1+m_1n_2 & l_2n_1+l_1n_2 & l_2m_1+l_1m_2 \end{bmatrix}$$

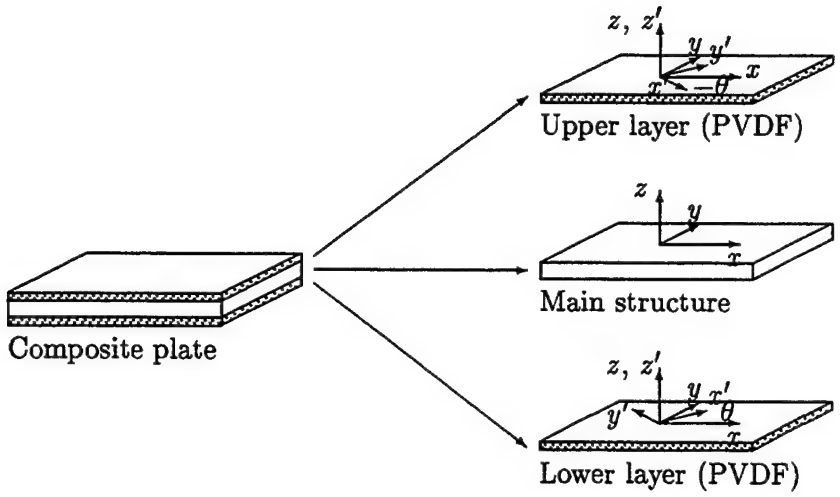

Figure 4: Skew Angle

$$[\mathbf{T}_s] = \begin{bmatrix} l_1^2 & m_1^2 & n_1^2 & m_1n_1 & n_1l_1 & l_1m_1 \\ l_2^2 & m_2^2 & n_2^2 & m_2n_2 & n_2l_2 & l_2m_2 \\ l_3^2 & m_3^2 & n_3^2 & m_3n_1 & n_3l_1 & l_3m_1 \\ 2l_2l_3 & 2m_2m_3 & 2n_2n_3 & m_2n_3+m_3n_2 & l_2n_3+l_3n_2 & l_2m_3+l_3m_2 \\ 2l_1l_3 & 2m_1m_3 & 2n_1n_3 & m_1n_3+m_3n_1 & l_1n_3+l_3n_1 & l_1m_3+l_3m_1 \\ 2l_2l_1 & 2m_2m_1 & 2n_2n_1 & m_2n_1+m_1n_2 & l_2n_1+l_1n_2 & l_2m_1+l_1m_2 \end{bmatrix}$$

$$\begin{aligned} l_1 &= cos\theta \quad & l_2 &= -sin\theta \quad & l_3 &= 0 \\ m_1 &= sin\theta \quad & m_2 &= cos\theta \quad & m_3 &= 0 \\ m_1 &= 0 \quad & m_2 &= 0 \quad & n_3 &= 0 \end{aligned}$$

Then Eq. 2 is expressed as

$$\{\mathbf{T}\} = [\bar{\mathbf{c}}]\{\mathbf{S}\} - [\bar{\mathbf{e}}]^T\{\mathbf{E}\} \tag{10}$$

$$\{\mathbf{D}\} = [\bar{\mathbf{e}}]\{\mathbf{S}\} + [\epsilon]\{\mathbf{E}\} \tag{11}$$

where

$$[\bar{\mathbf{c}}] = [\mathbf{T}_t]^{-1}[\mathbf{c}][\mathbf{T}_s], \quad [\bar{\mathbf{e}}] = [\mathbf{e}][\mathbf{T}_s]$$

It can be observed from Eq. 10 and Eq. 11, that the modified piezoelectric constant, $[\bar{e}]$ matrix has non-zero e_{36} entry. The torsional motion can be produced by this coefficient. As shown in Fig. 4, two layers, bottom and upper layers, with opposite skew angles are required to generate torque of the wing. The maximum shear strain, γ_{xy} can be obtained when the skew angles are $\frac{\pi}{4}$.

2.4 Modeling of Aerodynamic Pressure Distribution Generating Roll Maneuver

We now consider the modeling of aerodynamic pressure distribution on the flexible wing structure. According to piston theory [9][10] the aerodynamic pressure on the surface of a wing for a high Mach number ($\mathbf{M} > 1.6$) is expressed as

$$\Delta p = -\left[\lambda\left(\frac{\partial w}{\partial x}\right) + g\left(\frac{\partial w}{\partial t}\right)\right] \tag{12}$$

where

$$\lambda = \frac{2q}{(\mathbf{M}^2-1)^{0.5}}, \quad g = \frac{\lambda}{U_a}\frac{\mathbf{M}^2-2}{\mathbf{M}^2-1}, \quad q = \frac{1}{2}\rho_a U_a^2$$

ρ_a : *air density*

U_a : *air velocity*

Fig. 5 shows a 32 degrees of freedom brick element with aerodynamic loads. According to Eq. 12, these loads are changed by the vertical displacements of nodes and are assumed to act along the x coordinate. It is assumed that the pressure difference between upper and lower surfaces of the wing acts on the upper surface.

By substituting Eq. 4 into Eq. 12, the Eq. 12 can be rewritten as

$$\Delta p = -\lambda\,[\mathbf{N}_a]_{,\xi}\,\mathbf{q} \;-\; g\,[\mathbf{N}_a]\,\dot{\mathbf{q}} \tag{13}$$

where

$$[\mathbf{N}_a] = \begin{bmatrix} 0 & 0 & 0 & 0 & 0 & 0 & 0 & 0 & 0 & \cdots \\ 0 & 0 & 0 & 0 & 0 & 0 & 0 & 0 & 0 & \cdots \\ 0 & 0 & N_{1,\zeta=1} & 0 & 0 & N_{2,\zeta=1} & 0 & 0 & N_{3,\zeta=1} & \cdots \end{bmatrix}$$

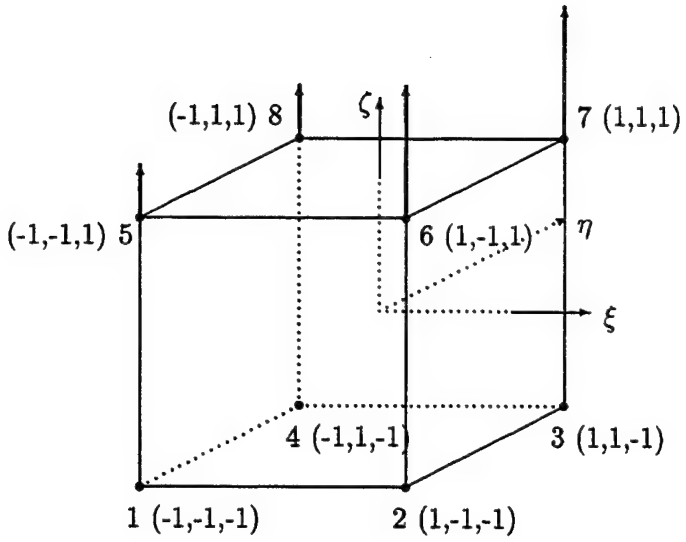

Figure 5: Coupled 8 Nodes 3-D Solid with Aerodynamic Load

2.5 Equation of Motion via Hamilton's Principle

The equation of motion of the wing can now be derived from Hamilton's principle which is expressed as

$$\int_{t_1}^{t_2} (\delta\mathcal{T} - \delta\mathcal{U})\ dt = 0 \tag{14}$$

where $\delta\mathcal{T}$ and $\delta\mathcal{U}$ are the first variation of kinetic energy and total potential energy including mechanical strain energy, electrical energy, and work done by externally applied forces and charge, respectively. Those energies are expressed as [11] [12]

$$\delta\mathcal{T} = \int_V \rho\dot{\mathbf{u}}\,\delta\dot{\mathbf{u}}\,dV \tag{15}$$

$$\begin{aligned}\delta\mathcal{U} \;=\; & \int_V \{\delta\{\mathbf{S}\}^T[\bar{\mathbf{c}}]\{\mathbf{S}\} - \delta\{\mathbf{S}\}^T[\bar{\mathbf{e}}]\{\mathbf{E}\} - \delta\{\mathbf{E}\}^T[\bar{\mathbf{e}}]^T\{\mathbf{S}\} - \delta\{\mathbf{E}\}^T[\epsilon]\{\mathbf{E}\}\}\,dV \\ & - \int_S (\mathbf{t}\,\delta\mathbf{u} - \mathbf{Q}\,\delta\varphi)\,dS\end{aligned} \tag{16}$$

where ρ,$\mathbf{u}$,$\mathbf{t}$, and $\mathbf{Q}$ are mass density, displacement vector, surface traction and surface charge, respectively. By substituting Eq. 15 and Eq. 16 into Eq. 14, the Hamilton's Principle with piezo-

electric material is expressed as

$$\int_V \{\delta\{\mathbf{S}\}^T[\bar{\mathbf{c}}]\{\mathbf{S}\} - \delta\{\mathbf{S}\}^T[\bar{\mathbf{e}}]\{\mathbf{E}\} - \delta\{\mathbf{E}\}^T[\bar{\mathbf{e}}]^T\{\mathbf{S}\} - \delta\{\mathbf{E}\}^T[\epsilon]\{\mathbf{E}\} + \rho\delta\dot{\mathbf{u}}^T\ddot{\mathbf{u}}\}\, dV - \int_S (\delta\mathbf{u}^T\mathbf{t} - \mathbf{Q}\,\delta\varphi)\, dS = 0 \tag{17}$$

By substituting Eq. 4 through 7 into Eq. 17, the Hamilton's Principle with the finite element method can be written as

$$\begin{aligned}\int_V & \{\delta\mathbf{q}^T[\mathbf{B}_q]^T[\bar{\mathbf{c}}][\mathbf{B}_q]\mathbf{q} + \delta\mathbf{q}^T[\mathbf{B}_q]^T[\bar{\mathbf{e}}]^T[\mathbf{B}_\varphi]\varphi + \delta\varphi^T[\mathbf{B}_\varphi]^T[\bar{\mathbf{e}}][\mathbf{B}_q]\mathbf{q} \\ & + \delta\varphi^T[\mathbf{B}_\varphi]^T[\epsilon][\mathbf{B}_\varphi]\varphi + \rho\delta\mathbf{q}^T[\mathbf{N}_q]^T[\mathbf{N}_q]\ddot{\mathbf{q}}\}\, dV \\ -\int_S & \{(\delta\mathbf{q}^T[\mathbf{N}_q]_{\zeta=1}^T(-\lambda[\mathbf{N}_a]_{,\xi}\mathbf{q} - g[\mathbf{N}_a]\dot{\mathbf{q}}) - \delta\varphi^T[\mathbf{N}_\varphi]^T\mathbf{Q}\}\, dS \\ = 0 & \end{aligned} \tag{18}$$

Eq. 18 can be reorganized as

$$\begin{aligned}\delta\mathbf{q}^T\{\int_V [\mathbf{B}_q]^T[\bar{\mathbf{c}}][\mathbf{B}_q]\,dV\,\mathbf{q} &+ \int_V [\mathbf{B}_q]^T[\bar{\mathbf{e}}]^T[\mathbf{B}_\varphi]\,dV + \int_V \rho[\mathbf{N}_q]^T[\mathbf{N}_q]\,dV\,\ddot{\mathbf{q}} \\ + \int_S g[\mathbf{N}_q]_{\zeta=1}^T[\mathbf{N}_a]\,dS\,\dot{\mathbf{q}} &+ \int_S \lambda[\mathbf{N}_q]_{\zeta=1}^T[\mathbf{N}_a]\,dS\,\mathbf{q}\} + \\ \delta\varphi^T\{\int_V [\mathbf{B}_\varphi]^T[\bar{\mathbf{e}}][\mathbf{B}_q]\,dV\,\mathbf{q} &+ \int_V [\mathbf{B}_\varphi]^T[\epsilon][\mathbf{B}_\varphi]\,dV\,\varphi \\ - \int_S [\mathbf{N}_\varphi]^T\mathbf{Q}dS\} &= 0 \end{aligned} \tag{19}$$

From Eq. 13, the aerodynamic loads are expressed in terms of the generalized coordinates of the element. Moreover, in Eq. 19, the loads are grouped as the stiffness and damping coefficient matrices of the system. These coefficients are labelled as aerodynamic stiffness and damping matrices. If Eq. 19 is rewritten in a matrix form, the well known Matrix Second Order System [13] can be obtained

$$\begin{bmatrix} M & 0 \\ 0 & 0 \end{bmatrix}\begin{bmatrix} \ddot{\mathbf{q}} \\ \ddot{\varphi} \end{bmatrix} + \begin{bmatrix} C_A & 0 \\ 0 & 0 \end{bmatrix}\begin{bmatrix} \dot{\mathbf{q}} \\ \dot{\varphi} \end{bmatrix} + \begin{bmatrix} K_q + K_A & K_{q\varphi} \\ K_{\varphi q} & K_{\varphi\varphi} \end{bmatrix}\begin{bmatrix} \mathbf{q} \\ \varphi \end{bmatrix} = \begin{bmatrix} 0 \\ \mathbf{Q} \end{bmatrix} \tag{20}$$

where

$$\begin{aligned} M &= \int_{-1}^{1}\int_{-1}^{1}\int_{-1}^{1} \rho[\mathbf{N}_q]^T[\mathbf{N}_q]\,|J|\,d\xi\,d\eta\,d\zeta \\ C_A &= \int_{-1}^{1}\int_{-1}^{1} g[\mathbf{N}_q]_{\zeta=1}^T[\mathbf{N}_a]\,|J_a|\,d\xi\,d\eta \end{aligned}$$

$$
\begin{aligned}
K_q &= \int_{-1}^{1}\int_{-1}^{1}\int_{-1}^{1} [\mathbf{B}_q]^T [\bar{\mathbf{c}}] [\mathbf{B}_q] |J| d\xi d\eta d\zeta \\
K_A &= \int_{-1}^{1}\int_{-1}^{1} \lambda [\mathbf{N}_q]_{\zeta=1}^T [\mathbf{N}_a] |J_a| d\xi d\eta \\
K_{q\varphi} &= \int_{-1}^{1}\int_{-1}^{1}\int_{-1}^{1} [\mathbf{B}_q]^T [\bar{\mathbf{e}}]^T [\mathbf{B}_\varphi] |J| d\xi d\eta d\zeta \\
K_{\varphi q} &= K_{q\varphi}^T \\
K_{\varphi\varphi} &= \int_{-1}^{1}\int_{-1}^{1}\int_{-1}^{1} [\mathbf{B}_\varphi]^T [\epsilon] [\mathbf{B}_\varphi] |J| d\xi d\eta d\zeta
\end{aligned}
$$

and J and J_a are the Jacobian matrices.

$$
J = \begin{bmatrix}
\frac{\partial N_1}{\partial \xi} & \frac{\partial N_2}{\partial \xi} & \frac{\partial N_3}{\partial \xi} & \frac{\partial N_4}{\partial \xi} & \frac{\partial N_5}{\partial \xi} & \frac{\partial N_6}{\partial \xi} & \frac{\partial N_7}{\partial \xi} & \frac{\partial N_8}{\partial \xi} \\
\frac{\partial N_1}{\partial \eta} & \frac{\partial N_2}{\partial \eta} & \frac{\partial N_3}{\partial \eta} & \frac{\partial N_4}{\partial \eta} & \frac{\partial N_5}{\partial \eta} & \frac{\partial N_6}{\partial \eta} & \frac{\partial N_7}{\partial \eta} & \frac{\partial N_8}{\partial \eta} \\
\frac{\partial N_1}{\partial \zeta} & \frac{\partial N_2}{\partial \zeta} & \frac{\partial N_3}{\partial \zeta} & \frac{\partial N_4}{\partial \zeta} & \frac{\partial N_5}{\partial \zeta} & \frac{\partial N_6}{\partial \zeta} & \frac{\partial N_7}{\partial \zeta} & \frac{\partial N_8}{\partial \zeta}
\end{bmatrix}
\begin{bmatrix}
x_1 & y_1 & z1 \\
x_2 & y_2 & z2 \\
x_3 & y_3 & z3 \\
x_4 & y_4 & z4 \\
x_5 & y_5 & z5 \\
x_6 & y_6 & z6 \\
x_7 & y_7 & z7 \\
x_8 & y_8 & z8
\end{bmatrix}
$$

$$
J_a = \begin{bmatrix}
\frac{\partial N_1}{\partial \xi} & \frac{\partial N_2}{\partial \xi} & \frac{\partial N_3}{\partial \xi} & \frac{\partial N_4}{\partial \xi} \\
\frac{\partial N_1}{\partial \eta} & \frac{\partial N_2}{\partial \eta} & \frac{\partial N_3}{\partial \eta} & \frac{\partial N_4}{\partial \eta}
\end{bmatrix}
\begin{bmatrix}
x_1 & y_1 \\
x_2 & y_2 \\
x_3 & y_3 \\
x_4 & y_4
\end{bmatrix}
$$

3 Equation of Steady Roll and the Corresponding Deformed Structural Vibration Model

Aircraft flight maneuvers are always accompanied by structural vibrations. In this research, specifically the roll maneuver with a constant roll rate and the resulting structural dynamic vibrations are analyzed. The structural dynamic deformations under the roll maneuver with a desired roll rate are modeled clearly as follows. Fig. 6 shows a plate wing with roll axis constraints.

3.1 Equation of Motion for Roll for Deformable Wing

The roll motion, generally, is expressed as an angular motion. The finite element model, however, is expressed in terms of generalized coordinates which are nodal displacements. So in this research, the roll angular motion is obtained by first modeling the deformation of the wing under steady state roll rate which in turn is achieved by steady state voltage actuation. Since, the model of the wing is expressed with nodal displacements and voltages, the angular displacement cannot be directly modeled in the generalized coordinates. The angular displacement of roll motion and its relationship to the input voltage can be obtained from the moment equilibrium equation of the wing. The roll equation of motion for a wing as shown in Fig. 7 is expressed as

$$I\ddot{\phi} = M_R \tag{21}$$

where

$I = \frac{1}{3}ml^2$: Moment of inertia

ϕ : Roll angle

M_R : Rolling moment due to lift

The rolling moment due to lift, M_R, is expressed as

$$M_R = \int_0^l L(y)dy \tag{22}$$

where $L(y)$ is lift force.

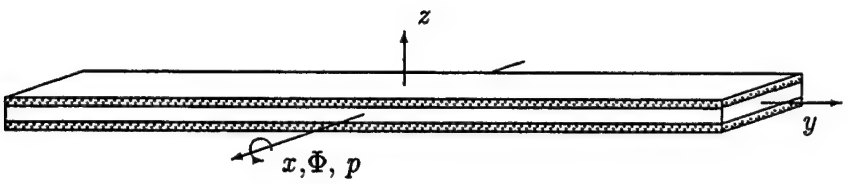

Figure 6: Wing Plate with Piezoelectric Lamina

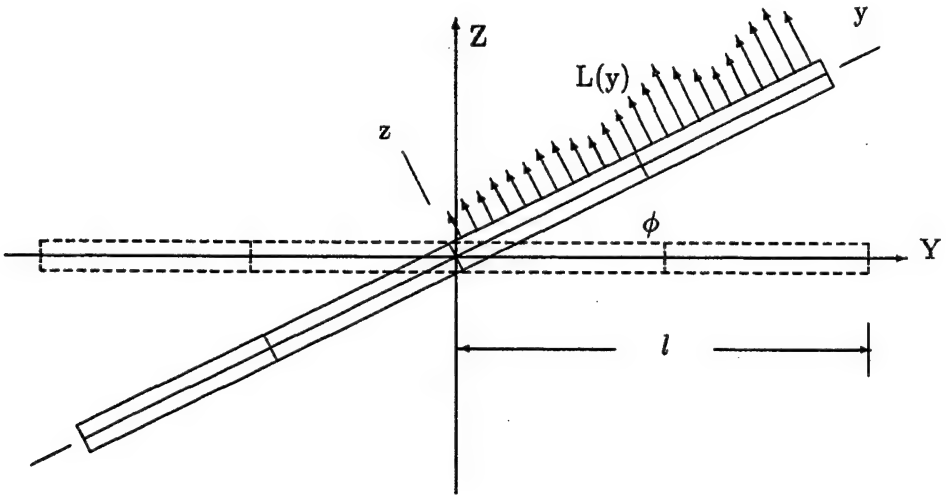

Figure 7: Roll Motion of a Wing

The lift, $L(y)$, is written as

$$L(y) = qcC_L(y) \tag{23}$$

where $q = \frac{\rho U^2}{2}$: dynamic pressure

ρ : air density

U : air velocity

c : airfoil span

$C_L(y)$: lift coefficient

The lift coefficient, $C_L(y)$, is can be expressed as a function of α, angle of attack

$$C_L(y) = \frac{\partial C_L(y)}{\partial \alpha} [\alpha_0(y) + \alpha_e(y)] \tag{24}$$

where $\alpha_0(y)$ and $\alpha_e(y)$ are angle of attack for zero lift and due to elastic twist. Note that, $\alpha_e(y)$ can be written as

$$\alpha_e(y) = \alpha_{pz}(y) - \frac{Py}{U} \tag{25}$$

where

$\alpha_{pz}(y)$:angle of attack produced by piezoelectric actuation

$\frac{Py}{U}$: Induced angle of attack due to roll rate 'P'.

By substituting Eq. 25 into Eq. 24, the lift coefficient is written as

$$C_L(y) = C_{L_\alpha} \left(\alpha_{pz}(y) - \frac{Py}{U} \right) \tag{26}$$

where $C_{L_\alpha} = \frac{\partial C_L(y)}{\partial \alpha}$.

By introducing Eq. 26 into Eq. 23, the lift is expressed as

$$\begin{aligned} L(y) &= C_{L_\alpha} qc \left(\alpha_{pz}(y) - \frac{Py}{U} \right) \\ &= \frac{C_{L_\alpha} \rho c U^2}{2} \left(\alpha_{pz}(y) - \frac{Py}{U} \right) \end{aligned} \tag{27}$$

Then, the rolling moment is obtained as

$$\begin{aligned} M_R &= \frac{C_{L_\alpha} \rho c U^2}{2} \int_0^l \left[\alpha_{pz}(y) - \frac{Py}{U} \right] dy \\ &= \frac{C_{L_\alpha} \rho c U^2}{2} \left[-\frac{Pl^2}{2U} + \int_0^l \alpha_{pz}(y) dy \right] \end{aligned} \tag{28}$$

By substitution Eq. 28 into Eq. 21 and using $P = \dot{\phi}$, the equation of motion for the roll can be expressed as

$$I\ddot{\phi} + \frac{C_{L_\alpha} \rho c U l^2}{4} \dot{\phi} = \frac{C_{L_\alpha} \rho c U^2}{2} \int_0^l \alpha_{pz}(y) dy \tag{29}$$

A finite element model analysis, as depicted in Fig. 8, is required in order to find the relationship between the angle of attack, $\alpha_{pz}(y)$, and the nodal voltage input, v. For the purpose of modeling, it is assumed that chordwise segments of the wing remain rigid. Fig. 9 shows the cross sectional area and angle of attack, α, of the wing. The angle α is the twisting angle due to the piezoelectric

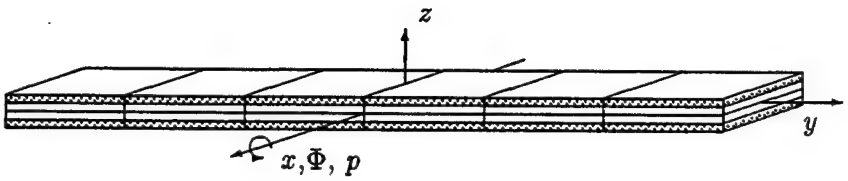

Figure 8: The Finite Element Model of the Wing Plate with Piezoelectric Lamina

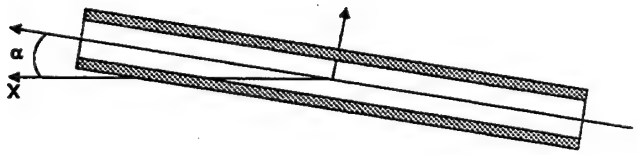

Figure 9: Cross-sectional area of a wing

actuation in the element local coordinates. First, the angle of attack in the element coordinates, $\alpha_{pz}(\eta)$ has to be obtained ($\alpha_{pz}(y) \Rightarrow \alpha_{pz}(\eta)$). From the assumption, the angle α is constant through the chord line for the small twist angle. Since the angle of attack is measured from the centerline of the cross section of the wing, the angle α is expressed as

$$\alpha(y) = \left.\frac{\partial w}{\partial x}\right|_{z=c_z} \tag{30}$$

where w and c_z is transverse displacement at nodes and z coordinate values of center line of the wing, respectively. In the element local coordinates, the angle α is expressed as

$$\alpha_{pz}(\eta) = \left.\frac{\partial w}{\partial \xi}\right|_{\zeta=c_\zeta} \tag{31}$$

where c_ζ is the coordinate value for centerline of the cross sectional area of the wing in the local coordinate. Finally, the angle α is expressed in the generalized coordinates as

$$\alpha_{pz}(\eta) = [L_{tw}]\,[N_q]\,q = [B_{tw}]\,q \tag{32}$$

where

$$\begin{aligned}
[L_{tw}] &= \left[\begin{array}{ccc} 0 & 0 & \left.\frac{\partial}{\partial \xi}\right|_{\zeta=c_\zeta} \end{array}\right] \\
[B_{tw}] &= \left[\begin{array}{ccccccccc} 0 & 0 & \left.\frac{\partial N_1}{\partial \xi}\right|_{\zeta=c_\zeta} & 0 & 0 & \left.\frac{\partial N_2}{\partial \xi}\right|_{\zeta=c_\zeta} & \cdots & 0 & 0 & \left.\frac{\partial N_8}{\partial \xi}\right|_{\zeta=c_\zeta} \end{array}\right] \\
[\mathbf{q}] &= \left[\begin{array}{ccccccccccc} u_1 & v_1 & w_1 & u_2 & v_2 & w_2 & \cdots & u_8 & v_8 & w_8 \end{array}\right]^T
\end{aligned}$$

To build full model, the angle of attack has to be integrated into the physical coordinates which is expressed as

$$\int_{y_1}^{y_2} \alpha_{pz}(y)dy \tag{33}$$

where y_1 and y_2 are lower and upper bound for the element in the y coordinate as shown in Fig. 10.

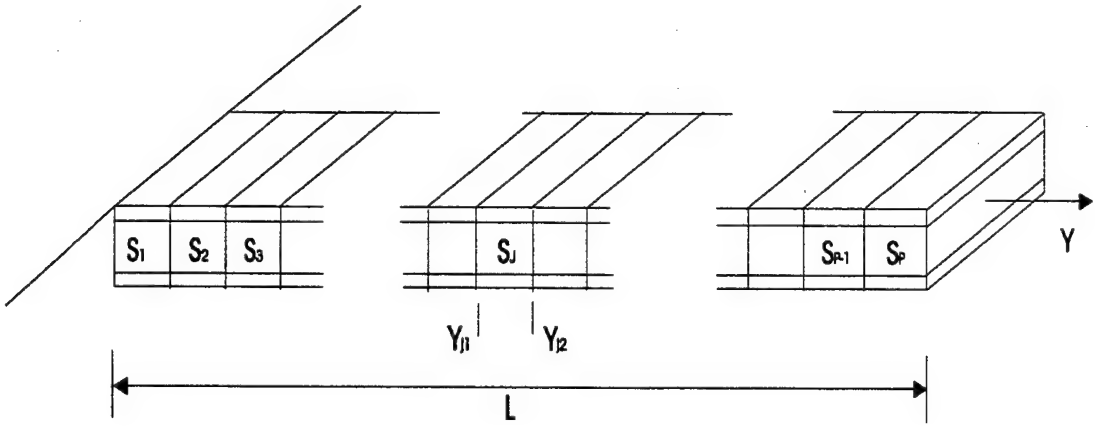

Figure 10: Finite element Model for a Wing

Since the twisting angle is constant throughout the chord line, ξ can be selected as zero. The modified shape function is expressed as

$$\mathcal{N}_i = \frac{1}{8}(1+\eta\eta_i)(1+c_\zeta\zeta_i) \tag{34}$$

The y coordinates are written as

$$y = \sum_{i=1}^{8} \mathcal{N}_i y_i. \tag{35}$$

From the chain rule

$$dy = \frac{dy}{d\eta}d\eta \tag{36}$$

$$\frac{dy}{d\eta} = \sum_{i=1}^{8} \frac{d\mathcal{N}_i}{d\eta} y_i \tag{37}$$

The angle of attack for the j^{th} structural element in the physical coordinate y is expressed as

$$\begin{aligned} \mathcal{A}_j &= \int_{y_1}^{y_2} \alpha_{pz}(y)dy \\ &= \int_{-1}^{1} \alpha_{pz}(\eta) \sum_{i=1}^{8} \frac{d\mathcal{N}_i}{d\eta} y_{j_i} d\eta \\ &= \int_{-1}^{1} [B_{tw}] \sum_{i=1}^{8} \frac{d\mathcal{N}_i}{d\eta} y_{j_i} d\eta q_j \\ &= [B_\alpha] J_{\alpha_j} q_j \end{aligned} \tag{38}$$

where

q_j : the generalized coordinates for j^{th} element

$[B_\alpha] = \left[\begin{array}{cccccccccc} 0 & 0 & \int_{-1}^{1} \frac{\partial N_1}{\partial \xi}\Big|_{\zeta=c_\zeta} d\eta & 0 & 0 & \int_{-1}^{1} \frac{\partial N_2}{\partial \xi}\Big|_{\zeta=c_\zeta} d\eta & \cdots & 0 & 0 & \int_{-1}^{1} \frac{\partial N_8}{\partial \xi}\Big|_{\zeta=c_\zeta} d\eta \end{array} \right]$

$J_{\alpha_j} = \sum_{i=1}^{8} \frac{d\mathcal{N}_i}{d\eta} y_{j_i} d\eta.$

Thus, the total integration of the angle of attack is written as

$$\int_0^l \alpha_{pz}(y)dy = \sum_{j=1}^{p} \mathcal{A}_j \tag{39}$$

$$= [B_{\alpha q}]\, q \tag{40}$$

where $[B_{\alpha q}]$ is the $(1 \times n)$ matrix which contains $[B_\alpha] J_{\alpha_j}$ for the corresponding nodal displacement q. The nodal displacement vector q can be expressed as function of voltage input from the equation

of motion of the cantilevered wing which is expressed as

$$[M_q]\,\ddot{q} + [K_q]\,q = -\,[K_{q\varphi}]\,v \tag{41}$$

where v is voltage input. Fig. 11 shows the twisting motion of a cantilevered wing with voltage actuation.

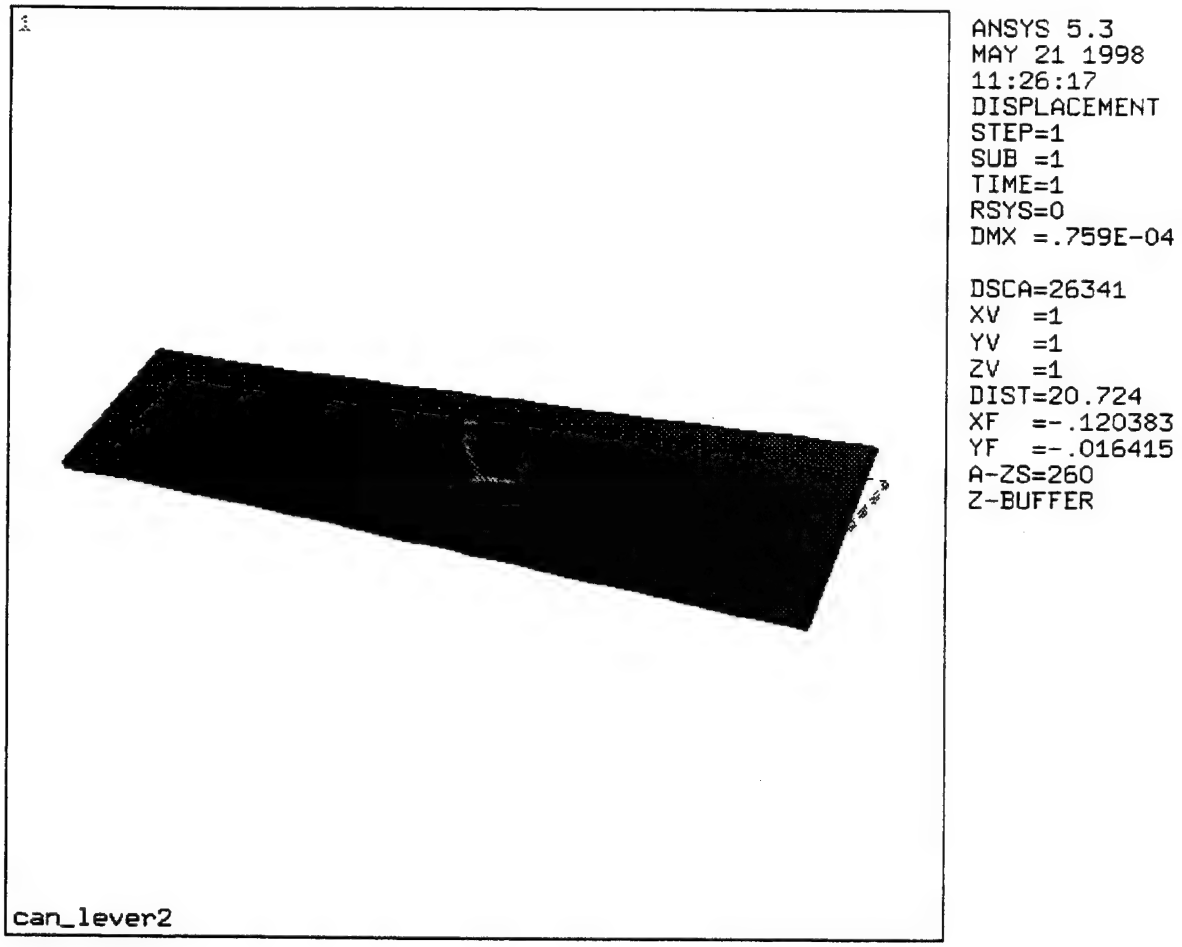

Figure 11: A Twisting Motion in a Cantilevered Wing

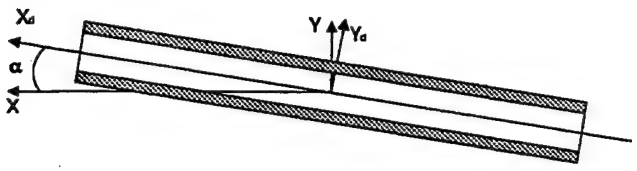

Figure 12: Deformed Coordinates

Since the twisting angle is the static deflection of the wing, Eq. 41 can be reduced to

$$[K_q]\, q = -[K_{q\varphi}]\, v_r \tag{42}$$

where v_r is voltage input for roll. Since the stiffness matrix of the cantilevered wing is not singular, the displacements are expressed as

$$\mathbf{q} = -[K_q]^{-1}\,[K_{q\varphi}]\, v_r \tag{43}$$

By substituting Eq. 43 into Eq. 29, the equation of motion for roll motion with voltage actuation is expressed as

$$I\ddot{\phi} + \frac{C_{L_\alpha}\rho c U l^2}{4}\dot{\phi} = -\frac{C_{L_\alpha}\rho c U^2}{2}\,[B_{\alpha q}]\,[K_q]^{-1}\,[K_{q\varphi}]\, v_r \tag{44}$$

3.2 Equation of Motion for Deformed Structure

The next task is to analyze the vibrational motion of the wing. Considerable amount of research exists on the vibration suppression of flexible structures [14][15][16]. However, there are actually not many studies undertaken for modeling vibrations associated with flight maneuvers. In a roll maneuver with flexible wing, deformation of the wing is essential to achieve the desired roll motion. If vibration control is designed based on the original equation of motion of the wing, Eq. 41, however, it is difficult to achieve the desired angle of attack and the desired roll rate. Therefore, a new equation of motion for the deformed structure is required to dissipate the vibration of the wing as well as to obtain the desired roll motion. For this, we first formulate the finite element model based on the deformed coordinates, x_d, y_d and z_d, as shown in Fig. 12. The displacement

fields are then written as

$$\mathbf{u_d} = [\mathbf{N}_q]\mathbf{q_d} \tag{45}$$

$$\varphi_\mathbf{d} = [\mathbf{N}_\varphi]\{v_d\} \tag{46}$$

where

$$[\mathbf{q}] = \begin{bmatrix} u_{d_1} & v_{d_1} & w_{d_1} & u_{d_2} & v_{d_2} & w_{d_2} & \cdots & u_{d_8} & v_{d_8} & w_{d_8} \end{bmatrix}^T$$

$$[\varphi] = \begin{bmatrix} V_{d_1} & V_{d_2} & \cdots & V_{d_8} \end{bmatrix}^T$$

The strain fields are expressed as

$$\mathbf{S_d} = [\mathbf{B}_q]\mathbf{q_d} \tag{47}$$

$$\mathbf{E_d} = [\mathbf{B}_\varphi]\mathbf{v_d} \tag{48}$$

To obtain the equation of motion for the deformed structure, the following physical coordinates are used.

$$\mathbf{X_d} = \mathbf{X} + q_I \tag{49}$$

where

$$[\mathbf{X_d}] = \begin{bmatrix} x_{d_1} & y_{d_1} & z_{d_1} & x_{d_2} & y_{d_2} & z_{d_2} & \cdots & x_{d_8} & y_{d_8} & z_{d_8} \end{bmatrix}^T$$

$$[\mathbf{X}] = \begin{bmatrix} x_1 & y_1 & z_1 & x_2 & y_2 & z_2 & \cdots & x_8 & y_8 & z_8 \end{bmatrix}^T$$

$$[\mathbf{q_I}] = \begin{bmatrix} q_{I_1} & q_{I_2} & \cdots & q_{I_8} \end{bmatrix}^T$$

From the original undeformed structure, the initial displacement, q_I, can be obtained as

$$\mathbf{q_I} = -[K_q]^{-1}[K_{q\varphi}]\,v_r \tag{50}$$

where v_r is voltage input for desired roll. By substituting Eq. 50 into Eq. 49, the deformed coordinates are expressed as

$$\mathbf{X_d} = \mathbf{X} - [K_q]^{-1}[K_{q\varphi}]\,v_r \tag{51}$$

Finally the equation of the motion for a deformed structure in the aerodynamic field is then given by

$$\begin{bmatrix} M_d & 0 \\ 0 & 0 \end{bmatrix} \begin{bmatrix} \ddot{\mathbf{q}}_\mathbf{d} \\ \ddot{\varphi} \end{bmatrix} + \begin{bmatrix} C_{A_d} & 0 \\ 0 & 0 \end{bmatrix} \begin{bmatrix} \dot{\mathbf{q}}_\mathbf{d} \\ \dot{\varphi} \end{bmatrix} + \begin{bmatrix} K_d + K_{A_d} & K_{q\varphi_d} \\ K_{\varphi q_d} & K_{\varphi\varphi_d} \end{bmatrix} \begin{bmatrix} \mathbf{q}_\mathbf{d} \\ \varphi \end{bmatrix} = \begin{bmatrix} 0 \\ \mathbf{Q}_\mathbf{d} \end{bmatrix} \quad (52)$$

where

$$\begin{aligned}
M_d &= \int_{-1}^{1}\int_{-1}^{1}\int_{-1}^{1} \rho \left[\mathbf{N}_q\right]^T \left[\mathbf{N}_q\right] |J_d| d\xi d\eta d\zeta \\
C_{A_d} &= \int_{-1}^{1}\int_{-1}^{1} g \left[\mathbf{N}_q\right]_{\zeta=1}^T \left[\mathbf{N}_a\right] |J_{a_d}| d\xi d\eta \\
K_d &= \int_{-1}^{1}\int_{-1}^{1}\int_{-1}^{1} \left[\mathbf{B}_q\right]^T \left[\bar{\mathbf{c}}\right] \left[\mathbf{B}_q\right] |J_d| d\xi d\eta d\zeta \\
K_{A_d} &= \int_{-1}^{1}\int_{-1}^{1} \lambda \left[\mathbf{N}_q\right]_{\zeta=1}^T \left[\mathbf{N}_a\right] |J_{a_d}| d\xi d\eta \\
K_{q\varphi_d} &= \int_{-1}^{1}\int_{-1}^{1}\int_{-1}^{1} \left[\mathbf{B}_q\right]^T \left[\bar{\mathbf{e}}\right]^T \left[\mathbf{B}_\varphi\right] |J_d| d\xi d\eta d\zeta \\
K_{\varphi q_d} &= K_{q\varphi_d}^T \\
K_{\varphi\varphi_d} &= \int_{-1}^{1}\int_{-1}^{1}\int_{-1}^{1} \left[\mathbf{B}_\varphi\right]^T \left[\epsilon\right] \left[\mathbf{B}_\varphi\right] |J_d| d\xi d\eta d\zeta
\end{aligned}$$

and J_d is the Jacobian matrix for the deformed structure.

$$J_d = \begin{bmatrix} \frac{\partial N_1}{\partial \xi} & \frac{\partial N_2}{\partial \xi} & \frac{\partial N_3}{\partial \xi} & \frac{\partial N_4}{\partial \xi} & \frac{\partial N_5}{\partial \xi} & \frac{\partial N_6}{\partial \xi} & \frac{\partial N_7}{\partial \xi} & \frac{\partial N_8}{\partial \xi} \\ \frac{\partial N_1}{\partial \eta} & \frac{\partial N_2}{\partial \eta} & \frac{\partial N_3}{\partial \eta} & \frac{\partial N_4}{\partial \eta} & \frac{\partial N_5}{\partial \eta} & \frac{\partial N_6}{\partial \eta} & \frac{\partial N_7}{\partial \eta} & \frac{\partial N_8}{\partial \eta} \\ \frac{\partial N_1}{\partial \zeta} & \frac{\partial N_2}{\partial \zeta} & \frac{\partial N_3}{\partial \zeta} & \frac{\partial N_4}{\partial \zeta} & \frac{\partial N_5}{\partial \zeta} & \frac{\partial N_6}{\partial \zeta} & \frac{\partial N_7}{\partial \zeta} & \frac{\partial N_8}{\partial \zeta} \end{bmatrix} \begin{bmatrix} x_{d_1} & y_{d_1} & zd_1 \\ x_{d_2} & y_{d_2} & zd_2 \\ x_{d_3} & y_{d_3} & zd_3 \\ x_{d_4} & y_{d_4} & zd_4 \\ x_{d_5} & y_{d_5} & zd_5 \\ x_{d_6} & y_{d_6} & zd_6 \\ x_{d_7} & y_{d_7} & zd_7 \\ x_{d_8} & y_{d_8} & zd_8 \end{bmatrix}$$

$$J_a = \begin{bmatrix} \frac{\partial N_1}{\partial \xi} & \frac{\partial N_2}{\partial \xi} & \frac{\partial N_3}{\partial \xi} & \frac{\partial N_4}{\partial \xi} \\ \frac{\partial N_1}{\partial \eta} & \frac{\partial N_2}{\partial \eta} & \frac{\partial N_3}{\partial \eta} & \frac{\partial N_4}{\partial \eta} \end{bmatrix} \begin{bmatrix} x_{d_1} & y_{d_1} \\ x_{d_2} & y_{d_2} \\ x_{d_3} & y_{d_3} \\ x_{d_4} & y_{d_4} \end{bmatrix}$$

4 Control Design Specifically Tailored to Smart Structural Systems

State space representation is a useful tool to design controllers for linear systems and many control design methods in state space framework are available for achieving stabilization and regulation of the state variables. However, for our particular problem at hand, namely, to achieve a desired constant roll rate, it turns out to be cumbersome to use state space based control design because the steady state constant roll rate implies infinite roll displacements as time progresses. Therefore, the closed loop system is considered unstable. To overcome this problem and still design a simple controller using available control system software for this desired roll rate achievement problem, we propose a new framework called the 'Reciprocal State Space' framework [17]. This is discussed in the next section.

4.1 Full State Derivative Feedback Control Design for Roll Motion using Reciprocal State Space Representation

The state space representation of Eq. 44 is expressed as

$$\begin{aligned}\begin{bmatrix}\dot{\phi}\\ \ddot{\phi}\end{bmatrix} &= \begin{bmatrix}0 & 1\\ 0 & -\frac{3C_{L_\alpha}\rho cU}{4m}\end{bmatrix}\begin{bmatrix}\phi\\ \dot{\phi}\end{bmatrix} + \begin{bmatrix}0\\ -\frac{3C_{L_\alpha}\rho cU^2}{2ml^2}\left[B_{\alpha q}\right]\left[K_q\right]^{-1}\left[K_{q\varphi}\right]\end{bmatrix} v_r\\ \dot{x_r} &= A_r x + B_r u\end{aligned} \tag{53}$$

where $x = \begin{bmatrix}\phi & \dot{\phi}\end{bmatrix}^T$.

The reciprocal state space representation of the system is expressed as

$$\begin{aligned}x &= G\dot{x} + Hu\\ u &= K\dot{x}\end{aligned} \tag{54}$$

where

$$G = A_r^{-1},\ \ H = -A_r^{-1}B_r$$

For regulation problem,

$$\begin{aligned}\dot{\xi} &= \dot{x} + \mathcal{P}\\ \xi &= x + \mathcal{V}\end{aligned} \tag{55}$$

where

$$\mathcal{P} = p_d$$

$$\mathcal{V} = p_d\, t$$

$$p_d \quad : \quad \textit{desired roll rates}$$

Then, Eq. 54 is written as

$$\dot{\xi} = G\xi + Hu \tag{56}$$

$$u = K\dot{\xi} \tag{57}$$

From Eq. 54, the performance index to be minimized is expressed as

$$J = \int_0^\infty \left[\dot{\xi}^T \mathcal{Q}\dot{\xi} + u^T \mathcal{R}u\right]\, dt \tag{58}$$

where $\mathcal{Q}$ and $\mathcal{R}$ are positive semidefinite matrix and positive definite matrix, respectively. According to references [18][19], the LQR state feedback gain is written as

$$K = \mathcal{R}^{-1}H^T S \tag{59}$$

The matrix S can be obtained from the associated Algebraic Matrix Riccati equation which is expressed as

$$0 = SG + G^T S - SH\mathcal{R}^{-1}H^T S + \mathcal{Q} \tag{60}$$

5 Model Reduction in Nonorthogonal Modal Coordinates for Deformed Structure

From Eq. 52, the equation of motion with voltage actuation is written as

$$M_d\ddot{\mathbf{q}} + C_{A_d}\dot{\mathbf{q}} + (K_d + K_{A_d})\mathbf{q} = -K_{q\varphi_d}v \tag{61}$$

By premultiplying M_d^{-1} for both side of Eq. 61, the Eq. 61 is expressed as

$$\ddot{\mathbf{q}} + M_d^{-1}C_{A_d}\dot{\mathbf{q}} + M_d^{-1}(K_d + K_{A_d})\mathbf{q} = -M_d^{-1}K_{q\varphi_d}v \tag{62}$$

The modal equation of motion of the system can be obtained with a similarity transformation that diagonalizes the integrated stiffness matrix [20].

Let

$$\mathbf{q} = T\eta \tag{63}$$

where

$$T = [t_1\ t_2\ t_3\ ...t_n] \quad t_i : eigen\ vector\ of\ M_d^{-1}(K_d + K_{A_d})$$

Then, Eq. 62 can be written as

$$\ddot{\eta} + C_\eta\eta + \Lambda\eta = F_\eta\varphi \tag{64}$$

where

$$\begin{aligned}
\eta &= [\eta_r\ \eta_{f1}\ \eta_{f2}\ ...] \\
C_\eta &= T^{-1}M_d^{-1}C_{A_d}T \\
\Lambda &= T^{-1}M_d^{-1}(K_d + K_{A_d})T = diag(\Lambda_r, \Lambda_{f1}, \Lambda_{f1}, ...) \\
F_\eta &= -T^{-1}M_d^{-1}K_{q\varphi_d}
\end{aligned}$$

But the model in this (nonorthogonal) modal coordinates is too large for meaningful control design. For this purpose, we carry out a transformation to the nonorthogonal (but real) modal

coordinates clearly identifying the roll mode and all the flexible modes. The corresponding state space form of Eq. 64 is written as

$$\begin{aligned}\begin{bmatrix}\dot{\eta}\\ \ddot{\eta}\end{bmatrix} &= \begin{bmatrix}0 & I\\ -\Lambda & -C_\eta\end{bmatrix}\begin{bmatrix}\eta\\ \dot{\eta}\end{bmatrix} + \begin{bmatrix}0\\ F_\eta\end{bmatrix}\varphi\\ \dot{x} &= Ax + Bu\end{aligned} \tag{65}$$

6 New Observer Design

The full state and state derivative feedback control design, which is presented in the previous section, is achievable only if every state and state derivative is measured. In real world, every state and its derivative, however, cannot be measured. As an example, the piezo-laminated aircraft structure in aerodynamic field provide only displacement information through piezoelectric sensors. Therefore, an estimator design is required to build a proper and useful controller.

The motion of the multi-disciplinary flexible aircraft structures, such as a piezo-laminated aircraft structure in aerodynamic field[5], can be expressed in the form of multi-variable MSO differential equations through the well-known finite element method. Traditionally, the MSO system is converted to the first order standard state-space. The rationale for this is as follows: firstly, it is easier to handle the first order state-space differential equation rather than the MSO differential equation, secondly, there are handful of valuable and reliable control design methods and stability theories in the state-space, and finally, any higher order linear differential equation can be converted to the linear first order state-space.

However, there are several unique problems associated with the standard technique of transforming the MSO system into a state-space framework. First of all, it is difficult to preserve the physical properties such as mass, stiffness and damping coefficients in the state-space framework. As seen before, a typical MSO differential equation is of the form.

$$M\ddot{q} + C\dot{q} + Kq = bf \tag{66}$$

where $M_{n\times n}$, $C_{n\times n}$ and $K_{n\times n}$ are mass, damping and stiffness matrices, respectively. $b_{n\times m}$ is actuator distribution matrix. $q_{n\times 1}$ and $f_{m\times 1}$ are generalized displacements and external forcing vectors, respectively. The state-space representation for above MSO differential equation is expressed as

$$\begin{aligned} \begin{bmatrix} \dot{q} \\ \ddot{q} \end{bmatrix} &= \begin{bmatrix} 0 & I \\ -M^{-1}K & -M^{-1}C \end{bmatrix} \begin{bmatrix} q \\ \dot{q} \end{bmatrix} + \begin{bmatrix} 0 \\ b \end{bmatrix} f \\ \dot{x} &= Ax + Bf. \end{aligned} \tag{67}$$

In the MSO system, Eq. 66, valuable information can be obtained by analyzing the coefficient matrices. For example, the quantities of mass, damping, and stiffness can be observed directly

from the coefficient matrices M, C and K. The orthogonality of the system also can be determined by looking at the symmetric configuration of M and K matrices.

However, this information cannot be directly obtained in the state space because the mass, damping, and stiffness coefficient matrices are mixed into the system matrix 'A' as shown in Eq. 67. Secondly, in the state-space, the system size becomes large [13] and it is difficult to apply acceleration feedback control design which is effective to minimize the control effort[17]. Moreover, the correct estimate values for the second order system cannot be obtained through the first order observer, which will be explained later.

The disadvantages of the first order control scheme can be eliminated by using the second order controller and observer design schemes as shown in the literatures[13][17]. Especially, the proper estimated values for the second order system can be achievable through the proposed second order observer design scheme. However, because of the special structure of the observer gain matrix of the second order observer, the observer does not obey the existing observability criteria. Therefore, in this study, a new necessary and sufficient condition for the introduced second order observer design is determined.

6.1 The Disadvantages of the First Order Observer

Introduced in late 1950's, the first order state-space control design technique has been very useful and important. The advantages of the state-space are that any higher order dynamic systems can be described by a set of the first order differential equations; it is easy to handle the multiple-input multiple-output (MIMO) system; and a number of stability and control theories exist. However, there are several problems to handle the second order system in the first order state-space as mentioned in the introduction part. The most significant problem among them is the mismatch of the estimated values for the velocity information, $\hat{\dot{q}}$ and $\dot{\hat{q}}$, in the first order observer design. The typical first order observer is written as

$$\begin{aligned}
\begin{bmatrix} \dot{\hat{q}} \\ \ddot{\hat{q}} \end{bmatrix} &= \begin{bmatrix} 0 & I \\ -M^{-1}K & -M^{-1}C \end{bmatrix} \begin{bmatrix} \hat{q} \\ \dot{\hat{q}} \end{bmatrix} + \begin{bmatrix} 0 \\ b \end{bmatrix} u - \begin{bmatrix} \kappa_1 \\ \kappa_2 \end{bmatrix} \begin{bmatrix} y - \hat{y} \end{bmatrix} \\
y &= Cx \\
\hat{y} &= C\hat{x}.
\end{aligned} \tag{68}$$

where κ_1 and κ_2 are the observer gain matrices. Subtract Eq. 68 from Eq. 67, then

$$\begin{bmatrix} \dot{q}-\dot{\hat{q}} \\ \ddot{q}-\dot{\hat{q}} \end{bmatrix} = \begin{bmatrix} 0 & I \\ -M^{-1}K & -M^{-1}C \end{bmatrix} \begin{bmatrix} q-\hat{q} \\ \dot{q}-\dot{\hat{q}} \end{bmatrix} + \begin{bmatrix} \kappa_1 \\ \kappa_2 \end{bmatrix} \begin{bmatrix} c_1 & c_2 \end{bmatrix} \begin{bmatrix} q-\hat{q} \\ \dot{q}-\dot{\hat{q}} \end{bmatrix} \tag{69}$$

Let, $e_1 = q - \hat{q}$ and $e_2 = \dot{q} - \dot{\hat{q}}$, then Eq. 69 is written as

$$\begin{bmatrix} \dot{e_1} \\ \dot{e_2} \end{bmatrix} = \begin{bmatrix} \kappa_1 c_1 & I + \kappa_1 c_2 \\ -M^{-1}K + \kappa_2 c_1 & -M^{-1}C + \kappa_2 c_2 \end{bmatrix} \begin{bmatrix} e_1 \\ e_2 \end{bmatrix} \tag{70}$$

From Eq. 70, $\dot{e_1} \neq e_2$ unless $\kappa_1 = 0$, which is usually not zero in the first order observer. As a result, the unique values for $\dot{\hat{q}}$ and $\ddot{\hat{q}}$ cannot be obtained through the first order observer. The differences between $\hat{q}$ and $\dot{\hat{q}}$ are easily observed if Eq. 68 is rewritten as

$$\begin{aligned} \dot{\hat{q}} &= \hat{q} + \kappa_1 \left[y - \hat{y} \right] \\ \ddot{\hat{q}} &= -M^{-1}C\hat{q} - M^{-1}K\hat{q} + bu + \kappa_2 \left[y - \hat{y} \right] \end{aligned} \tag{71}$$

6.2 The Proposed 'Natural' Second Order Observer

The disadvantages of the first order control scheme can be eliminated by using the second order controller and observer design schemes as shown in the literatures[13][17]. Especially, the unique $\dot{\hat{q}}$ can be achievable through the introduced second order observer design scheme. The introduced observer design scheme is written as

$$\begin{aligned} M\ddot{\hat{q}} + C\dot{\hat{q}} + K\hat{q} &= bf - L_v(y_v - \hat{y}_v) - L_d(y_d - \hat{y}_d) \\ y_v = H_v\dot{q}, &\qquad y_d = H_d q \\ \hat{y}_v = H_v\dot{\hat{q}}, &\qquad \hat{y}_d = H_d\hat{q}. \end{aligned} \tag{72}$$

where L_v and L_d are the observer gain matrices. H_v and H_d are the sensor distribution matrices. From Eq. 72, the unique estimate values of the velocity information can be obtained through the second order observer. It is more clearly shown when the observer is written as the first order state-space form. The state-space form of the second order observer is expressed as

$$\begin{aligned} \begin{bmatrix} \dot{\hat{q}} \\ \ddot{\hat{q}} \end{bmatrix} &= \begin{bmatrix} 0 & I \\ -M^{-1}K & -M^{-1}C \end{bmatrix} \begin{bmatrix} \hat{q} \\ \dot{\hat{q}} \end{bmatrix} + \begin{bmatrix} 0 \\ M^{-1}b \end{bmatrix} f + \begin{bmatrix} 0 & 0 \\ L_dH_d & L_vH_v \end{bmatrix} \begin{bmatrix} q-\hat{q} \\ \dot{q}-\dot{\hat{q}} \end{bmatrix} \\ \dot{\hat{x}} &= A\hat{x} + Bf + G\underline{e} \end{aligned} \tag{73}$$

where

$$\hat{x} = \begin{bmatrix} \hat{q} & \hat{\dot{q}} \end{bmatrix}^T$$
$$\underline{e} = \begin{bmatrix} q-\hat{q} & \dot{q}-\hat{\dot{q}} \end{bmatrix}^T$$

According to Eq. 73, the two partition matrices, G_{11} and G_{12}, which are equivalent to κ_1 in the first order observer in Eq. 68, are inherently zero in the second order observer while κ_1 is usually not zero in the first order observer. Because of these zero gain matrices, the partition matrices A_{11} and A_{12} of system matrix A in the state-space remain as zero and identity matrices in the closed loop error dynamics. In other words, the characteristics of the second order dynamic are preserved in the second order observer design. The above Eq. (73) can be reorganized as

$$\begin{bmatrix} \dot{e} \\ \ddot{e} \end{bmatrix} = \left(\begin{bmatrix} 0 & I \\ -M^{-1}K & -M^{-1}C \end{bmatrix} + \begin{bmatrix} 0 \\ I \end{bmatrix} \begin{bmatrix} L_d & L_v \end{bmatrix} \begin{bmatrix} H_d & 0 \\ 0 & H_v \end{bmatrix} \right) \begin{bmatrix} e \\ \dot{e} \end{bmatrix}$$
$$\dot{\underline{e}} = (A+FLH)\underline{e} \tag{74}$$

where

$$A = \begin{bmatrix} 0 & I \\ -M^{-1}K & -M^{-1}C \end{bmatrix} (2n \times 2n)$$
$$F = \begin{bmatrix} 0 \\ I \end{bmatrix} (2n \times n)$$
$$L = \begin{bmatrix} L_d & L_v \end{bmatrix} (n \times 2n)$$
$$H = \begin{bmatrix} H_d & 0 \\ 0 & H_v \end{bmatrix} (2n \times 2n).$$

$\underline{e} = \begin{bmatrix} e & \dot{e} \end{bmatrix}^T$. The determination of gain 'L' follows the output feedback control design scheme.

7 Illustrative Example for Roll and Vibration Control

A PVDF plate wing with 2 layers and 16 elements, as shown in Fig. 13, is considered for control design whose objective is to achieve a desired constant roll rate as well as to suppress flexible mode vibrations. Each layer has opposite skew angle to generate torque of the wing. One half of the plate has eight 8-node brick elements with the total number of nodes being 30. In other words, the system has 120 degree of freedom, 90 for structural and 30 for electrical degrees of freedom. It is observed that the open loop system is unstable. Usually, a pure structural system is neutrally stable. But, the structure in the aerodynamic field is no longer stable because of the presence of the nonconservative aerodynamic field which contributes some stiffness as well as damping. By applying the proposed control design technique, the closed loop system is not only stabilized but also a desired constant roll rate of 1.5 rad/sec is achieved. Fig. 14 shows, for a selected set of weighting matrices, the roll rate responses. From this figure, it is clear that the desired roll velocity of 1.5 rad/sec is achieved by the controller. The corresponding roll angles are shown in Fig. 15. The roll angle gradually increases as expected. Fig. 16 shows the input voltage for the roll maneuver. The input voltage is used to build the deformed structure model. The rest of the flexible mode responses for the deformed structure are shown in Fig. 17, Fig. 18 and Fig. 19. It is easily seen that all flexible mode vibrational motion is suppressed effectively.. Fig. 20 shows the control input voltage histories at the node-2.

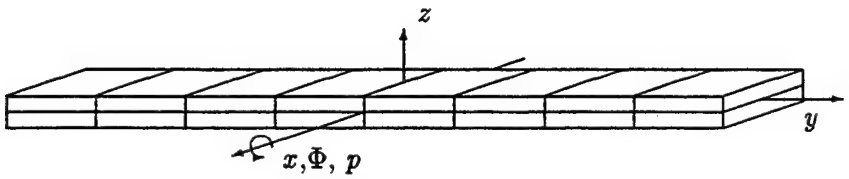

Figure 13: Wing Plate (PVDF)

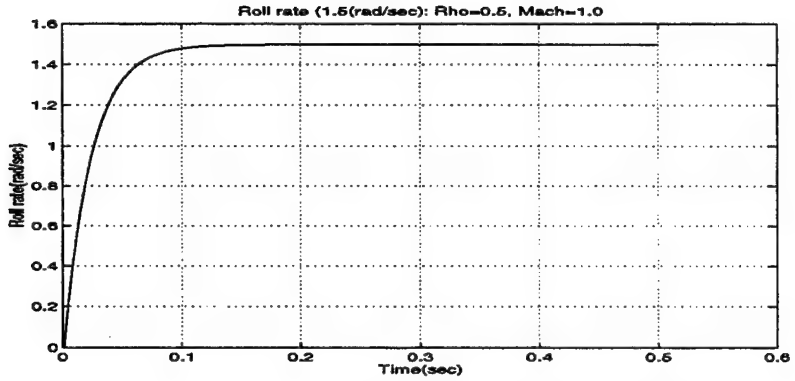

Figure 14: Roll Rate Response

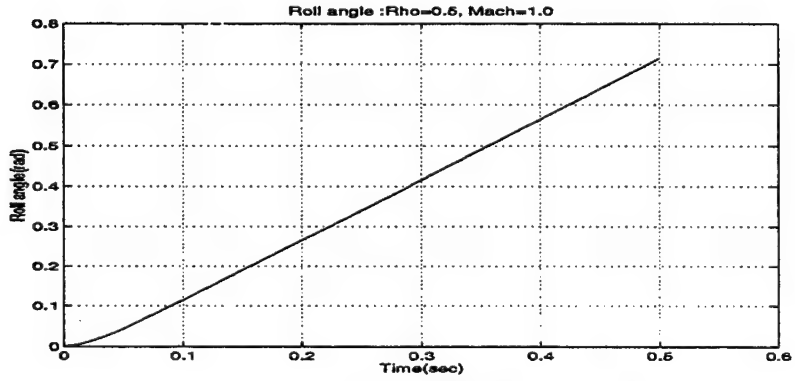

Figure 15: Roll Angle Response

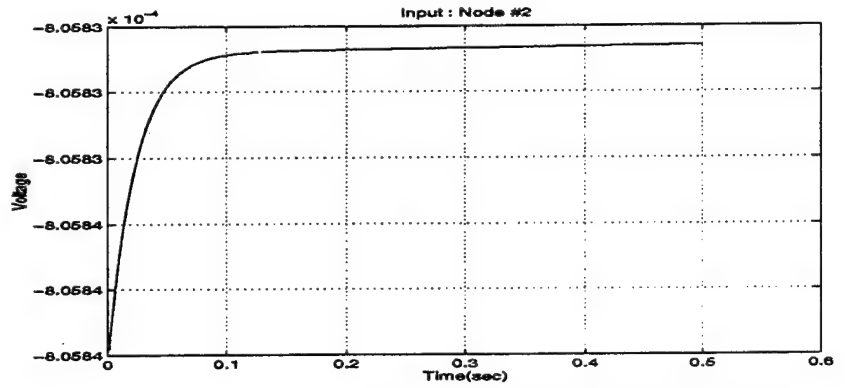

Figure 16: Input for Roll:Node 2 .

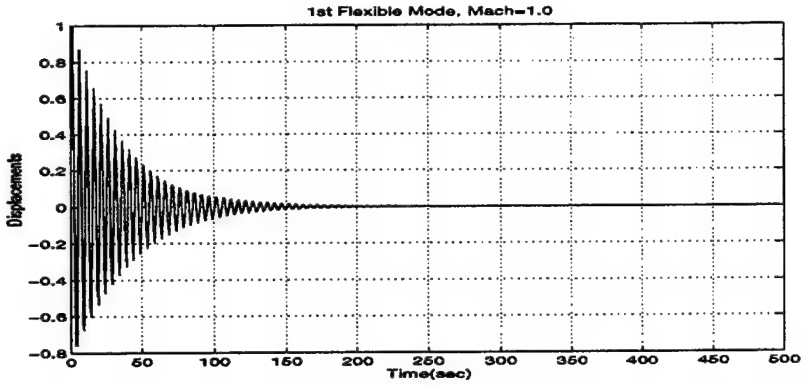

Figure 17: Displacement Response : 1st Flexible Mode

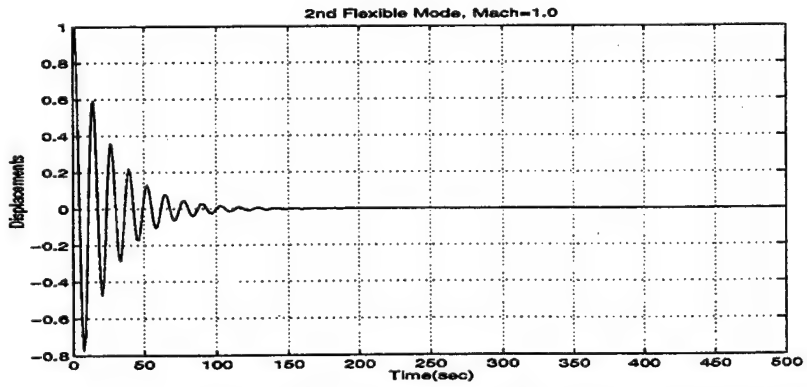

Figure 18: Displacement Response : 2nd Flexible Mode

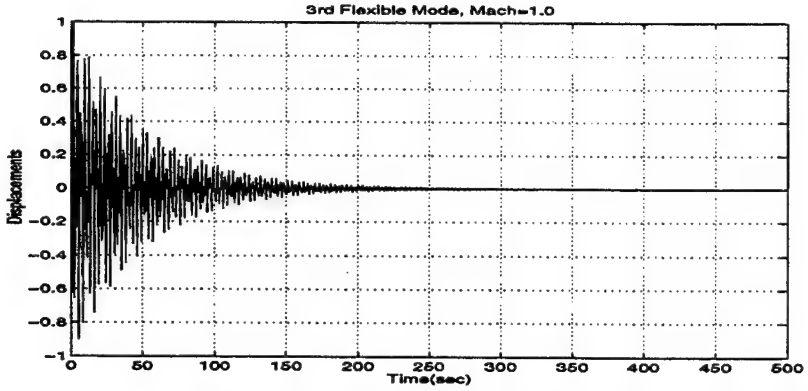

Figure 19: Displacement Response : 3rd Flexible Mode

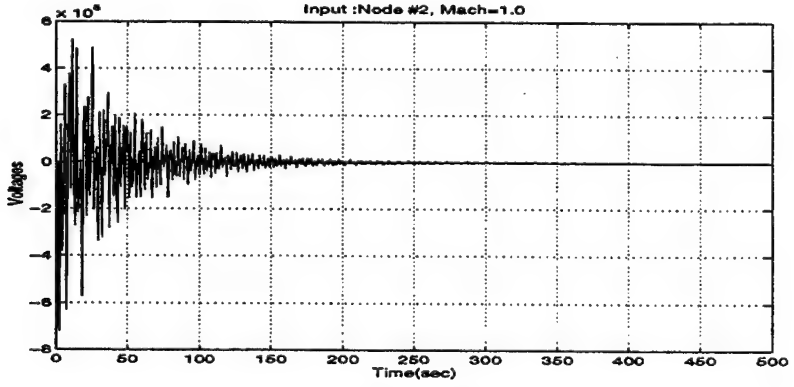

Figure 20: Input at Node 2

8 Conclusions:

In this research, an attempt is made, perhaps for the first time, to model the dynamics of a smart flexible wing involving the integration of five disciplines, namely structures, aerodynamics, smart materials, control and flight mechanics! The control objective is to sustain a roll maneuver with a desired roll rate and to suppress the flexible mode vibrations by actively deforming the wing. Modeling of this dynamics is done using finite element method in the 'generalized ' coordinates. Because of the coupling between these subsystems, the resulting 'Matrix Second Order System' of equations consists of a symmetric positive definite mass matrix but a nonsymmetric and indefinite damping (which includes aerodynamic damping) and stiffness (that includes aerodynamic and piezo material stiffness, in addition to the standard structural stiffness) matrices! The piezoelectric voltage serves as the control variables. The voltage dependent mass, stiffness, and damping matrices are also determined to maintain the desired roll rate during the roll maneuver. The roll control is designed in a new framework called 'Reciprocal State Space' framework which allows to implement acceleration feedback control easily. For the vibration problem, the large model in the generalized coordinates is then transformed to a set of 'nonorthogonal modal' coordinates and model reduction is carried out in these modal coordinates. This model is then converted to the 'state space' form and a controller is designed to supress the vibration using standard state space control theory. However, realizing that this full order controller is not practically achievable because all the desired states for feedback control cannot always be measured, an observer is sought. Finally, the observer based controller design is illustrated with the help of an example.

8.1 Future Research That Needs Support:

There is clearly a need to carry out further research in the following important areas. Firstly, more research should be undertaken to come up with improved control design algorithms, in the lines of present research proposed in this report. Secondly, the traditional integrated optimization ideas need to be expanded to include the interactions between the five subdisciplines mentioned before. Last, but not least, is the need to continue the analytical studies such as those presented in this report to more general flight maneuvers involving not only roll but pitch and yaw motions as well, and also a combination of these maneuvers using smart deformable wings. Of course, in

addition to analytical studies, considerable effort should be expended in conducting application studies to realistic scenarios involving software and hardware issues for industrial structures such as real wings. Finally, the importance of conducting experimental studies to validate the theories cannot be overemphasized. Thus, a long term commitment for research in 'Flight Control with Smart Deformable Wing Structures' must be of high priority for Universities such as The Ohio State University and Air Force (WL) and Aircraft Industries to reap the benefits of this exciting research.

9 References

[1] J.Kudva, K.Appa, C. Martin, and P.Jardine et al. Design, fabrication and testing of the darpa/wl smart wing wind tunnel model. *38th AIAA SDM Meeting*, April 1997.

[2] C.L.Hustedde, G.W.Reich, M.A.Hopkins, and K.E. Griffin. An investigation of the aeroelastic tailoring for smart structures concept. *37th AIAA SDM Meeting*, April 1996.

[3] N.S.Khot, F.E.Eastep, and R.M. Kolonay. Optimization of a composite wing structure for enhancement of the rolling maneuver. *AIAA-96-3998-CP*, 6th AIAA/NASA/USAF Multidisciplinary Analysis and Optimization Symposium, September 1996.

[4] N.S.Khot, F.E.Eastep, and R.M. Kolonay. Wing twist and camber for the rolling maneuver of a flexible wing without ailerons. *38th AIAA SDM Meeting*, April 1997.

[5] R. K .Yedavalli, N. S Khot, and S. K. Kwak. Improved aircraft roll maneuver performance using smart deformable wings. *Proceedings of SPIE 5th International Symposium on Smart Structures and Materials, San Diego*, 3323:55–66, March 1998.

[6] K. Appa and N. S. Khot et. al. Feasibility assessment and optimization study of smart actuation systems for enhanced aircraft maneuver performance. *WL-TR-97-3083*, July 1997.

[7] H. S. Tzou. Piezoelectric shell; distributed sensing and control of continua. *Solid Mechanics and Its Applications, Kluwer Academic Pub.*, 19, 1993.

[8] C.-K. Lee and F. C. Moon. Laminated piezopolymer plates for torsion and bending sensors and actuators. *Journal of Acoustical Society of America*, 85(6):2432–2439, June 1989.

[9] Holt Ashley and Garabed Zartarian. Piston theory - a new aerodynamic tool for the aeroelastician. *Journal of Aeronautical Sciences*, 23:1109–1118, December 1956.

[10] Maher N. Bismarck-Nasr. Finite element analysis of aeroelasticity of plates and shells. *Applied Mechanics Reviews*, 45(12, part 1):461–482, December 1992.

[11] H. S. Tzou and J. P. Zhong. Electromechanics and vibrations of piezoelectric shell distributed systems. *Transaction of the ASME*, 115:506–517, September 1993.

[12] Henno Allik and Thomas J. R. Hughes. Finite element method for piezoelectric vibration. *International Journal for Numerical methods in Engineering*, 2:151–157, 1970.

[13] Anjali M. Diwekar and Rama K. Yedavalli. Smart structure control in matrix second-order form. *Journal of Smart Structures and Materials*, 5:429–436, 1996.

[14] M. W. Obal S. Hanagud and A. J. Calise. Optimal vibration control by the use of piezoceramic sensors nad actuators. *AIAA Journal of Guidance, Control, and Dynamics*, 15(5):1199–1206, Sep.-Oct. 1992.

[15] Thomas Bailey and James E. Hubbard. Distributed piezoelectric-polymer active vibration control of a cantilever beam. *Journal of Guidance*, 8(5):605–611, Sep.-Oct. 1985.

[16] C.-C. Cheong S.-B. Choi and C.-H. Lee. Position tracking control of a smart flexible structure featuring a piezofilm actuator. *AIAA Journal of Guidance, Control, and Dynamics*, 19(6):1364–1369, Nov.-Dec. 1996.

[17] Yuan-Wei Tseng and R.K.Yedavalli. Control design of linear dynamic system with matrix differential equations for equations for aerospace applications. *Ph.D Dissertation*, The Ohio State University, 1997.

[18] Donald E. Kirk. Optimal control theory. *Prentice-Hall, Inc.*, 1970.

[19] Brian L. Stevens and Frank L. Lewis. Aircraft control and simulation. *JOHN WILEY and SONS, INC.*, 1992.

[20] L. Meirovitch. Computational methods in structural dynamics. *Sijthoff & Noordooff*, 1980.